Water-Soluble Iron Oxide Nanocubes with High Values of Specific Absorption Rate for Cancer Cell Hyperthermia Treatment

Pablo Guardia,[†] Riccardo Di Corato,[†,‡] Lenaic Lartigue,[§] Claire Wilhelm,[§] Ana Espinosa,[⊥] Mar Garcia-Hernandez,[⊥] Florence Gazeau,[§] Liberato Manna,[†] and Teresa Pellegrino[†,‡,*]

[†]Istituto Italiano di Tecnologia, via Morego 30, 16163 Genova, Italy, [‡]National Nanotechnology Laboratory of CNR-NANO, via per Arnesano km 5, 73100 Lecce, Italy, [§]Laboratoire Matière et Systèmes Complexes (MSC), UMR 7057, CNRS and Université Paris Diderot, 10 rue Alice Domon et Léonie Duquet, 75205 Paris cedex 13, France, and [⊥]Instituto de Ciencia de Materiales de Madrid, Consejo Superior de Investigaciones Científicas, Cantoblanco, 28049 Madrid, Spain

ABSTRACT

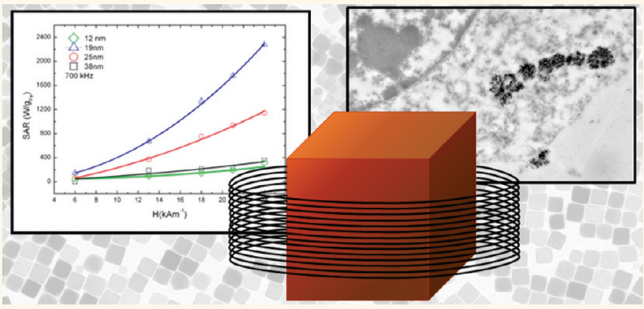

Iron oxide nanocrystals (IONCs) are appealing heat mediator nanoprobes in magnetic-mediated hyperthermia for cancer treatment. Here, specific absorption rate (SAR) values are reported for cube-shaped water-soluble IONCs prepared by a one-pot synthesis approach in a size range between 13 and 40 nm. The SAR values were determined as a function of frequency and magnetic field applied, also spanning technical conditions which are considered biomedically safe for patients. Among the different sizes tested, IONCs with an average diameter of 19 ± 3 nm had significant SAR values in clinical conditions and reached SAR values up to 2452 W/g$_{Fe}$ at 520 kHz and 29 kAm^{-1}, which is one of the highest values so far reported for IONCs. *In vitro* trials carried out on KB cancer cells treated with IONCs of 19 nm have shown efficient hyperthermia performance, with cell mortality of about 50% recorded when an equilibrium temperature of 43 °C was reached after 1 h of treatment.

KEYWORDS: hyperthermia treatment · specific absorption rate · SAR values · iron oxide nanoparticles · magnetic nanoparticles · biomedical applications · magnetosome-like nanoparticles

Magnetic nanoparticles (MNPs) provide a valuable platform with potential exploitation in biomedicine. MNPs have been proposed as magnetic guidance in drug delivery and magnetic separation, as contrast agents in magnetic resonance imaging (MRI), or as heat mediators in hyperthermia treatments.[1−4] The latter represents a novel therapeutic concept to cancer treatment and is based on the evidence that cancer cells are more sensitive than healthy cells to temperatures higher than 41 °C.[5,6] Among the various approaches proposed to raise the body temperature,[7−9] magnetically mediated hyperthermia is based on the generation of heat *via* an oscillating magnetic field exploiting MNPs as heating *foci*. MNPs can offer several advantages: (i) the nanoscale size of the heat probe would allow for their intravenous injection and their delivery *via* the bloodstream to tumors that could not be reached otherwise; (ii) the high surface to volume ratio of the MNPs allows for surface tailoring with few or multiple recognition molecules, which can guarantee targeting toward specific tumor tissues; (iii) the remote heating of MNPs by the externally applied magnetic field allows the heat action only to the zone of accumulation of nanoparticles.

The heating ability of MNPs under an alternating magnetic field is expressed by the specific absorption rate (SAR) which provides a measure of the rate at which energy is absorbed per unit mass of the magnetic material (the nanoparticles in this case) when exposed to a radio frequency.[10] The heat generation results either from hysteresis losses or from Néel or Brown relaxation processes.[5,11] SAR values depend on the structure and composition of the nanoparticles but also on the frequency (f) and the amplitude of the magnetic field (H) applied during the measurements.[11] For an efficient heat treatment with minimal invasiveness for the patient, the search for new magnetic nanomaterials which show the

* Address correspondence to teresa.pellegrino@iit.it.

Received for review December 9, 2011 and accepted March 16, 2012.

10.1021/nn2048137

highest SAR values at the lowest MNP dose administered and at the lowest frequency and/or magnetic field amplitude applied is of paramount relevance.[12,13] For superparamagnetic nanoparticles, SAR values usually increase by increasing either the frequency or the magnetic field amplitude (or both) applied during the measurements. Moreover, for a safe application of hyperthermia to patients, it was experimentally found that the product of the frequency and the magnetic field amplitude (*Hf*) should be smaller than 5×10^9 $Am^{-1}s^{-1}$.[12] First clinical trials were reported by applying 110 kHz and a field below 20 kAm^{-1}(in this case, the product *Hf* is clearly below that threshold).[14,15] However, many of the SAR values reported for magnetic nanoparticles are measured at frequencies between 500 and 700 kHz and fields between 10 and 20 kAm^{-1}, resulting in *Hf* factors which are mostly above this limit.[10,11,16,17] Moreover, the lack of standard devices or established measurement protocols[18] contributes to an increase of the variability of SAR values reported in the literature for MNPs.[5]

Hergt *et al.* hypothesized that higher SAR values might be achieved in the transition size range from superparamagnetic to ferromagnetic nanoparticles, which in the case of iron oxide nanocrystals (IONCs) should be around 20 nm.[5,19−21] Furthermore, for "injectable" nanoprobes, superparamagnetic nanoparticles should be preferred to ferromagnetic ones: the absence of any residual magnetization for those nanoparticles in the absence of the external applied magnetic field allows for a better dispersion and avoids the aggregation problems typical of ferromagnetic materials.[22,23] It should be considered that, in addition to the low SAR values of currently available superparamagnetic nanoparticles, also a drastic decrease of the heating power was observed whenever the superparamagnetic nanoparticles were localized into cells or tissues.[21,24,25] To overcome this limitation and reach a reasonable increase in temperature, higher doses and higher frequencies have been used in *in vitro* studies,[6,15] overcoming however the safety limits of the *Hf* factor.

Among the different materials that have shown promising magnetic properties (high saturation magnetization, relatively moderate anisotropy constant K_{eff}, and high initial susceptibility),[26−28] IONCs are by far the most studied ones also because of their biocompatibility and availability. IONCs indeed can be prepared by simple methods, like sol−gel or co-precipitation techniques, in large batches, and they were already launched in the first clinical hyperthermia trials.[2,15,29] On the other hand, most of the SAR studies were carried out on IONCs prepared using sol−gel or co-precipitation methods[23,30] showing a considerable polydispersity[31,32] which according to the theory could compromise the heating power.[33] In nature, magnetotactic bacteria[5,34] can produce IONCs in the size range of 20−50 nm, consisting of individual IONCs enwrapped within a membrane bilayer, so-called "magnetosomes". They exhibit high saturation magnetization and high crystallinity,[34] and for magnetosomes with a mean core diameter of 30 nm, the highest SAR values so far recorded were measured.[21,35]

A recent approach to the synthesis of MNPs is represented by thermal decomposition methods, and only few studies have reported SAR measurements of MNPs prepared by these methods. These yield nearly monodisperse NPs with sizes up to 15 nm,[32,36] but it appears more difficult to prepare IONCs with bigger sizes. Recently, Lartigue *et al.*[37] reported SAR values of sugar-coated IONCs synthesized by different colloidal methods[38−40] with sizes ranging between 4 and 35 nm. Their IONCs displayed good magnetic properties, and the largest IONCs prepared *via* thermal annealing of FeO nanoparticles[40] showed the highest hyperthermia performance. In another study, Levy *et al.*[41] reported on the SAR values of IONCs, with size in the range between 6 and 18 nm and with a control over the nanocrystal polydispersity below 2%, by refining a previously published seed-mediated growth approach.[39] Despite the high quality of the nanocrystals, the recorded SAR values were low. By a deeper magnetic and structural study, their behavior appeared to be a consequence of their magnetic core/shell structure consisting of a magnetic core, with size corresponding to that of the starting seed, surrounded by a magnetically frustrated layer.[41] This study suggested that such a seeded growth approach to prepare larger nanocrystals might not be the most suitable one if good hyperthermia performances are requested.

Herein, we report a study of the hyperthermia performance of IONCs prepared by a one-pot synthesis method capable of yielding nanocrystals in a size range between 12 and 40 nm and with a cube shape. For IONCs with a cube edge of 19 nm, we recorded the highest SAR values so far reported, and cell hyperthermia experiments conducted on particles of that size confirmed their efficacy even when taken up by the cells and under magnetic field parameters that are safe for patients. The results reported here contribute to fill the gap in SAR data of colloidal IONCs with size above 15 nm.

RESULTS AND DISCUSSION

Cube-shaped IONCs with cube edge lengths of 12 ± 1, 19 ± 3, 25 ± 4, and 38 ± 9 nm were synthesized by following a recently developed colloidal synthesis route and modified by us in order to achieve higher reproducibility (Figure 1).[42] Briefly, iron acetylacetonate and decanoic acid were mixed in dibenzyl ether. After degassing the solution for usually 45 min at room temperature, the temperature was increased to 200 °C and kept at this value for 2.5 h, and finally, it was

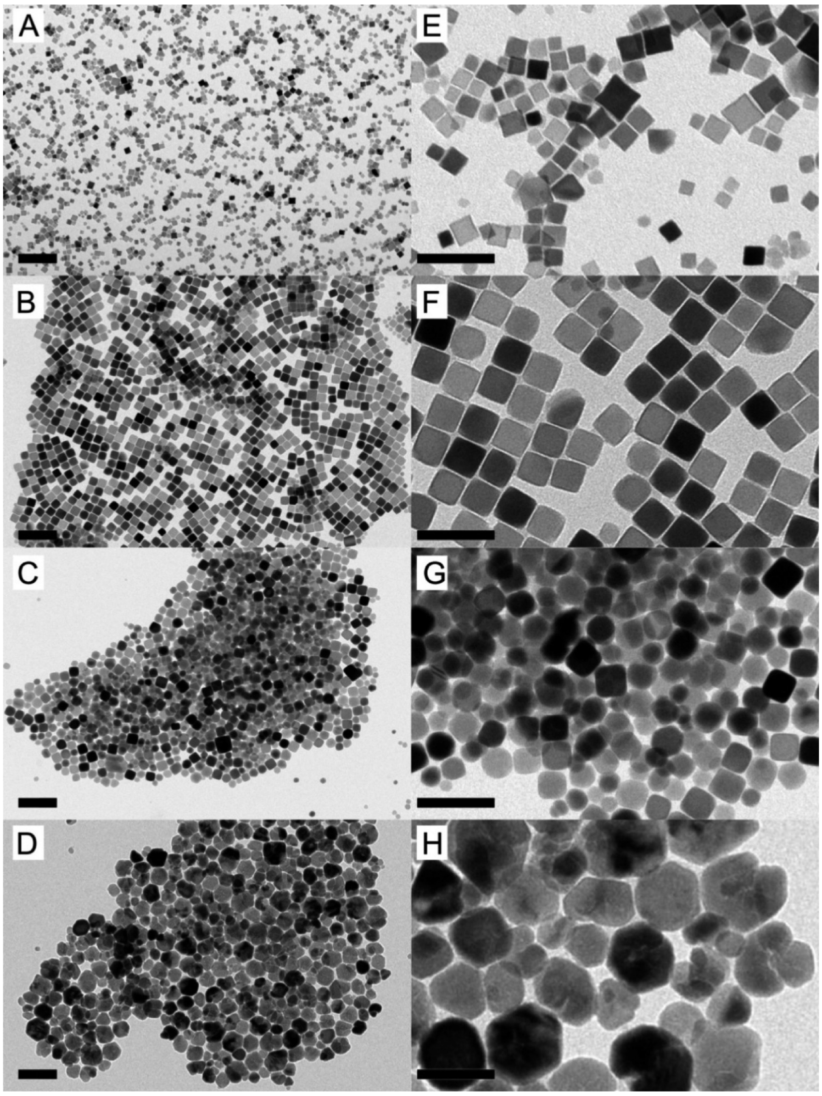

Figure 1. Representative transmission electron microscopy (TEM) images at low (left panel) and higher (right panel) magnification of "as-synthesized" iron oxide nanocubes for cube edge lengths of (A) 12 ± 1 nm, (B) 19 ± 3 nm, (C) 25 ± 4 nm, and (D) 38 ± 9 nm. Regular nanocubes could be obtained especially for 19 and 25 nm nanoparticle sizes. Panels E–H correspond to the TEM images at high magnification of the samples shown in panels A–D, respectively (scale bars correspond to 100 nm for A, B, C, and D and 50 nm for E, F, G, and H).

increased up to reflux (5 °C/min) and kept at this value for an additional 60 min, after which the flask was cooled to room temperature. The nanocrystals were then collected by precipitation with acetone followed by centrifugation at 8000 rpm. Various parameters were found to be critical for tuning the size and the shape of the nanocrystals: the decanoic acid/acetylacetonate ratio, the time of the vacuum step (using a standard rotary pump at 0.1 mbar) that was applied to the solution prior to the synthesis, as well as the heating rate when increasing the temperature from 200 °C up to reflux. For example, nanocrystals of 19 nm cube edge size were prepared by three repeated degassing cycles, for a total time of 45 min at room temperature, and working at a heating rate of 10 °C/min. Larger particles instead were prepared by following the same procedure with the only differences being either a slower heating rate (6 or 4 °C/min) or a slightly modified degassing step (see the Experimental Section for more details).

The surfactant-coated IONCs were transferred in water by using an amphiphilic polymer, namely, poly(maleic anhydride *alt*-1-octadecene), following a well-established procedure.[43] The alkyl chains of the polymer intercalate with the chains of the surfactants bound at the nanocrystal's surface, while the anhydride rings hydrolyze and ensure colloidal stability by means of electrostatic repulsions.[43] Henceforth, we will refer to these polymer-coated nanocrystals as "PC-IONCs". For nanocubes with size below 13 nm, no difficulties were encountered when applying the reported water solubilization procedure, while samples with sizes above 15 nm were characterized by strong interparticle magnetic interactions (see Figure 2B),

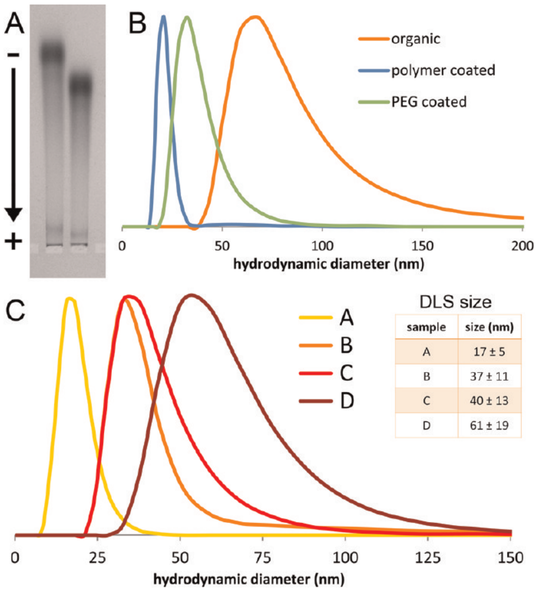

Figure 2. Characterization of IONCs in water. (A) Gel electrophoresis migration on 1% agarose gel at 100 V for 1 h of 19 nm IONCs, after polymer coating (left line) and subsequent monoamino-PEG functionalization (right line). (B) Comparison of the DLS profile for the same IONCs dispersed in chloroform (orange curve), after polymer coating (light blue curve), and finally after additional modification with monoamino-PEG (green curve). This sample was then used in the *in vitro* cellular study. (C) DLS diameters measured for water-soluble polymer-coated IONCs of TEM sizes corresponding to (A) 12 ± 1 nm, (B) 19 ± 3 nm, (C) 25 ± 4 nm and (D) 38 ± 9 nm.

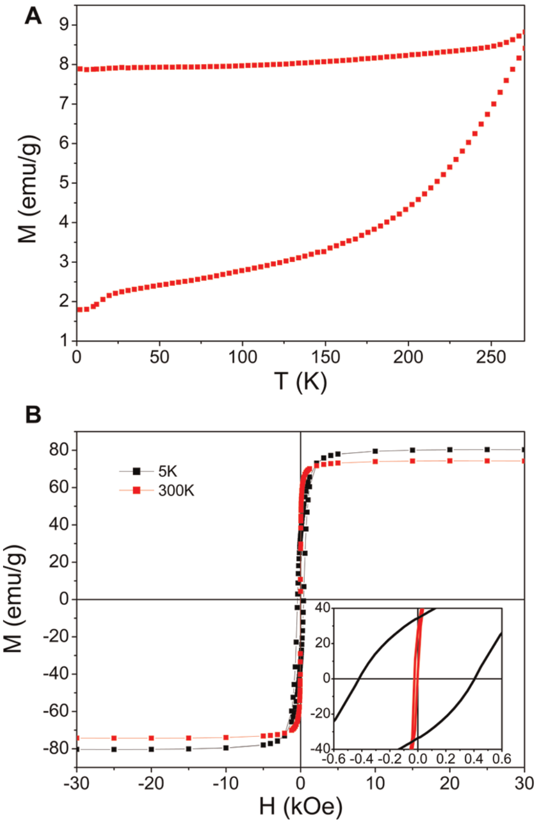

Figure 3. SQUID magnetization measurements performed on aqueous suspension of 19 nm PC-IONCs at a concentration of iron of 10 mM. (A) Zero field cooled/field cooled curves for an applied field of 5 mT; (B) field dependence of the magnetization at 5 K (black) and 310 K (red) as a function of the magnetic field strength. Inset: detail of the low field region to evaluate the coercive field.

which made the standard polymer coating procedure unsuccessful. To minimize particle–particle interactions, we worked with 10-fold more diluted solutions than in the standard protocol and, after mixing the IONCs with the polymer, the evaporation of the chloroform was performed quite slowly at 70 °C and at atmospheric pressure (against the evaporation at 40 °C and under reduced pressure of the standard protocol). Finally, the dried nanoparticles were dispersed in sodium buffer solution (50 mM, pH 9), and an ultrasonication step was applied to facilitate the dissolution of the nanoparticles into aqueous solution.

In this respect, it is worth comparing the hydrodynamic diameters measured by dynamic light scattering (DLS) of PC-IONCs of 19 nm in water with those of the same IONCs in the organic phase (Figure 2B). In the organic phase, due to stronger interparticle interactions, the DLS profile of IONCs is much broader and is peaked at a higher mean value than that corresponding to PC-IONCs in water. The presence of negatively charged carboxylic groups at the surface of the PC-IONCs helps them to repel each other, and thus smaller DLS sizes are found in water. Further functionalization of these particles is feasible without compromising the quality of the IONCs (Figure 2B). Monoamino(polyethyleneglycol (PEG)) molecules were linked to the IONC surface *via* EDC chemistry and, in accordance with the presence of longer spacer molecules, bigger diameters were measured for these PEG-coated IONCs (henceforth referred to as "PEG-IONCs"), while still preventing nanoparticles from aggregation (as seen from the narrow DLS peak in Figure 2B). Moreover, the gel electrophoresis migration of the PC-IONCs and PEG-IONCs toward the positive pole confirmed their high colloidal stability (Figure 2A).

The average maxima of DLS sizes for the different water-soluble PC-IONCs increased with increasing TEM size (from 12 to 38 nm) and corresponded to the expected diameters of individually coated IONCs. For the IONCs of 25 and 38 nm, the DLS peaks were instead much broader (Figure 2C), and therefore we cannot exclude for those samples the presence of small aggregates of two to three IONCs enwrapped together within the same polymer shell. In any case, what is remarkable is that by the modified polymer coating procedure it is possible to transfer in water IONCs of diameters below 20 nm, and these particles stay well dispersed and stable in solution. TEM images of the PC-IONCs in water also evidenced the presence of a thin shell of polymer around each individual nanoparticle and the absence of aggregates (the IONCs always formed a monolayer on the TEM grid; see Figure S1 of the Supporting Information).

The magnetic measurements performed on PC-IONCs in water confirmed high saturation magnetization values (M_S) ranging from 78 up to 95 emu/g. For instance, 19 nm PC-IONCs showed a saturation magnetization of 80 emu/g (Figure 3). The coercive field at 5 K of the nanocrystals with size below 20 nm is of the order of 400−500 Oe and suddenly decreases to 250−300 Oe for larger particles due to the transition from monodomain to multidomain regime, in good agreement with the recently reported data for the as-prepared cube-shaped IONCs in organic solution.[36,44] These data indicate the bulk-like behavior of IONCs synthesized by thermal decomposition, which was not observed so far on IONCs synthesized by co-precipitation.[45]

From magnetization curves at room temperature performed on a dilute water solution of PC-IONCs ([Fe] = 10 mM) of 19 nm, we measured a coercivity field of 415 Oe at 5 K, whereas no hysteresis was observed at room temperature. The thermal dependence of the magnetization upon field cooling (FC) and zero field cooling (ZFC) indicated that the blocking temperature is not far from 270 K but clearly higher than that. The measurements were voluntary stopped at 270 K, since beyond this temperature the water becomes liquid, leading to the onset of Brownian relaxation in addition to the Nèel internal relaxation (see also Figure S2 for the comparison with the magnetization curves on powder of IONPs of 19 nm). These data suggest that the IONCs with a mean size of 19 nm at room temperature are in the transition regime between superparamagnetism and ferrimagnetism.

In order to evaluate the hyperthermia performance on these water-soluble IONCs, the SAR value was measured by using a previously described homemade device (see Experimental Section).[16] Samples were exposed to different oscillating magnetic field amplitudes (from 2.3 up to 30 kAm^{-1}, depending on the frequency) at three different frequencies (320, 520, and 700 kHz). SAR values normalized to the iron amount, expressed as W/g$_{\mathrm{Fe}}$, were calculated according to the following equation:

$$\mathrm{SAR}\left(\frac{W}{g}\right) = \frac{C}{m} \times \frac{\mathrm{d}T}{\mathrm{d}t}$$

where C is the specific heat capacity of water per unit volume and m is the concentration (g/L of Fe) of magnetic material in solution. The sample holder temperature was kept at 37 °C, and the measurements were carried out in nonadiabatic conditions, thus the slope of the curve dT/dt was measured by taking into account only the first few seconds. Figure 4 reports the measured SAR values (expressed in W/g$_{\mathrm{Fe}}$ as a function of the frequency and strength of the applied magnetic field for the four samples of IONCs of different sizes). It is clear that the highest SAR values are recorded for IONCs of 19 nm in size. These particles had actually the highest SAR values at all of the applied frequencies, while either smaller or bigger particles were characterized by lower SAR values (Figure 4B). Interestingly, this most performing sample is the one on which the best control over shape and size distribution (with a polydispersity below 20%) was achieved during the synthesis. The 19 nm IONCs were found to reach a SAR value of 2277 W/g$_{\mathrm{Fe}}$ at 700 kHz and 24 kAm^{-1} and 1000 W/g at 325 kHz and 22 kAm^{-1}, almost the highest values recorded so far for iron oxide nanocrystals.[16,37]

As expected, for all of the IONP samples, higher SAR values were recorded by increasing the applied frequency, according to a linear trend (Figure 4A). A square dependence was also observed whenever at a fixed frequency the SAR values were plotted as a function of the applied magnetic field (Figure 4C,D and Figure S3).

Worthy of note is that the linear SAR dependence as a function of frequency and the quadratic SAR dependence as a function of applied magnetic field amplitude observed by us on cube-shaped IONCs have been theoretically predicted for spherical superparamagnetic IONCs[10,16] (see Supporting Information for the fitting of the experimental SARs based on the linear response theory). We might also speculate that the effective anisotropy deduced by the fit of the SAR as a function of magnetic field for the 19 and 25 nm nanocubes, equal to 4.4×10^4 and 2.4×10^4 erg cm^{-3}, respectively (see Figure S6), could account for their high magneto-thermal properties, as it was recently highlighted by Lee *et al.*[13] Indeed, in the linear response theory model, 22 nm spherical nanoparticles with low effective anisotropy (around 5×10^4 erg cm^{-3}) present the best heating properties.[10,16] The nanocubes with an edge length of 19 nm, having a comparable volume to that of 22 nm spherical nanoparticles, are therefore the sample that best matches this optimal size. To summarize, size and anisotropy of nanocubes of 19 nm, and to a lesser extent of 22 nm, are both in the favorable range to have high SAR values. Instead, the 13 and 38 nm nanocubes are not in this size range, and this might explain their relatively lower magneto-thermal properties.

Moreover, these recorded trends, combined with the high SAR values for our IONCs, suggest that increasing the amplitude of the magnetic applied field could be more advantageous than increasing the frequency in order to obtain higher SAR values. For example, in the case of 19 nm IONCs, a SAR value of 420 W/g was achieved at 700 kHz and 10 kAm^{-1}. The SAR increased up to 875 W/g by lowering the frequency by more than a factor of 2 (to 320 kHz) while keeping the Hf factor constant.

It is also remarkable that these IONCs exhibit significant SAR values even when the frequency and the

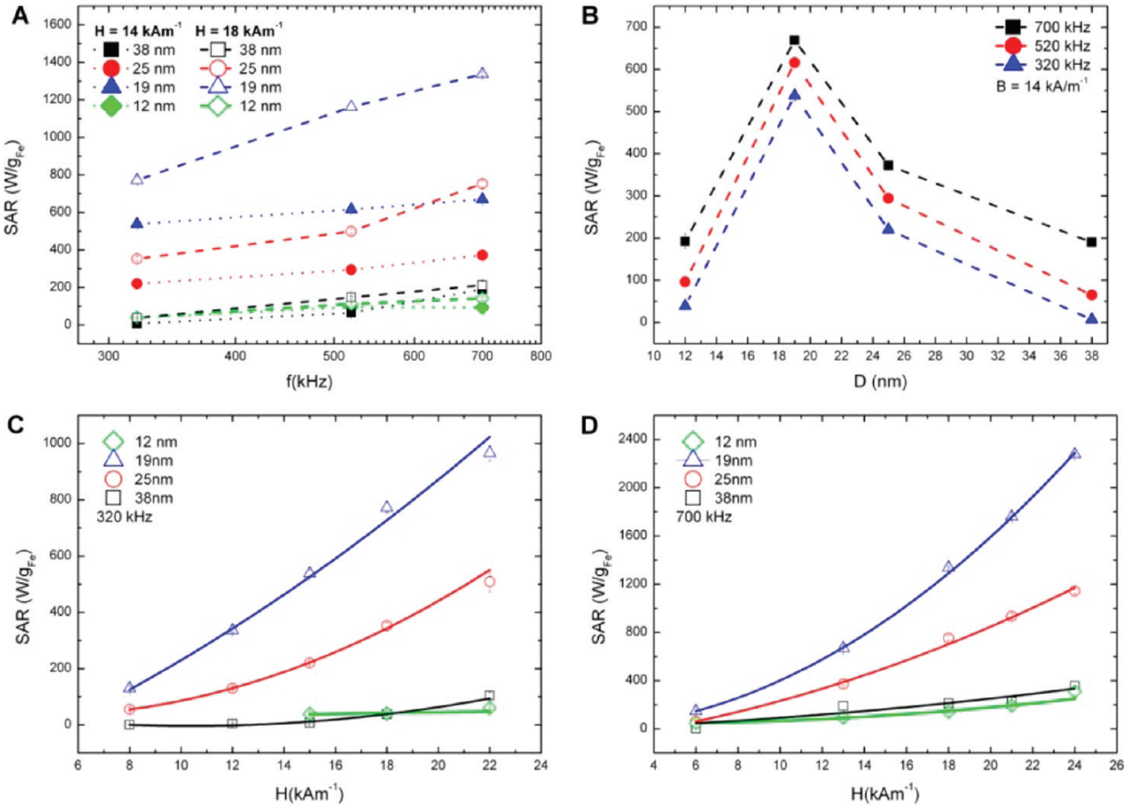

Figure 4. SAR values as a function of (A) frequency at the two magnetic field amplitudes of, respectively, 14 kAm^{-1} (solid symbols) and 18 kAm^{-1} (open symbols) for IONCs sizes equal to 12 ± 1 nm (green diamonds), 19 ± 3 nm (blue triangles), 25 ± 4 nm (red circles), and 38 ± 9 nm (black squares). (B) SAR values as a function of the size for frequencies of, respectively, 320 kHz (blue triangles), 520 kHz (red circles), and 700 kHz (black squares). (C,D) Magnetic field amplitude applied at a frequency of, respectively, 320 and 700 kHz. For the plots in (C,D), the symbols correspond to IONCs of 12 ± 1 nm (open green diamonds), 19 ± 3 nm (open blue triangles), 25 ± 4 nm (open red circles), and 38 ± 9 nm (open black squares). Each experimental data point was calculated as the mean value of at least four measurements, and error bars indicate the mean deviation. The solid lines represent the fits using linear response theory. Details for the fitting as well the deduced relaxation times are summarized in the Supporting Information.

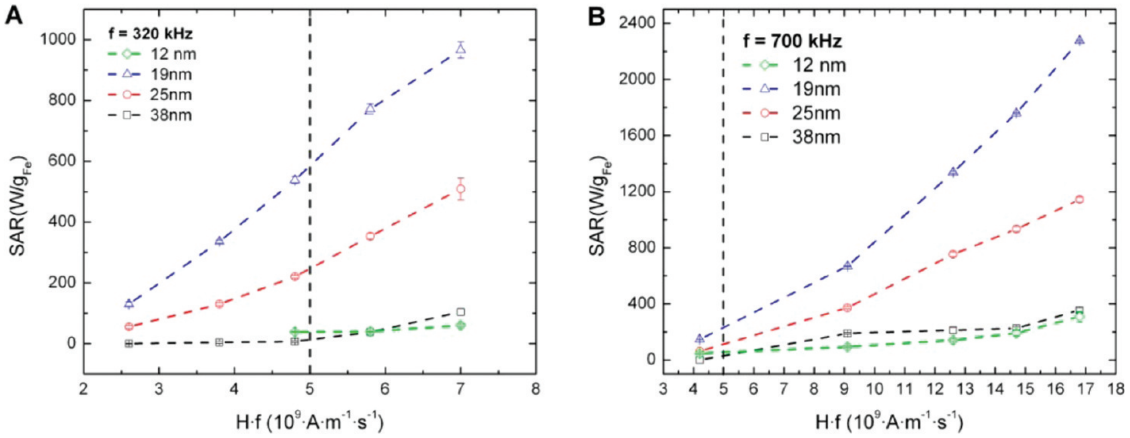

Figure 5. (A) SAR values as a function of the *Hf* factor at 320 kHz for IONCs of sizes equal to, respectively, 12 nm (open green rhombs), 19 nm (open blue triangles), 25 nm (open red circles), and 38 nm (open black squares). (B) SAR values as a function of the *Hf* factor for 19 nm iron oxide nanocubes at frequencies of 320 kHz (open blue triangles), 520 kHz (open red circles), and 700 kHz (open black squares). Experimental SAR values were calculated as the mean values of at least four measurements, and error bars indicate the mean deviation (in some cases, they are so small that they are not visible). The black line defines the biological limit for the *Hf* factor that is generally accepted as biologically safe.

magnetic field amplitudes are within values that are considered safe for patients, that is, when the product *Hf* is below 5 × 10^9 Am^{-1}s^{-1}, especially for the measurements recorded by applying different magnetic field amplitudes at a fixed frequency of 320 kHz (Figure 5; see also Figure S4). Working at lower frequencies clearly has the advantage that many different values of the applied magnetic field can be chosen such that the *Hf* factor is below the threshold, while working at higher frequencies restricts the choice of the possible magnetic field applied: for example, in the case of 19 nm size IONCs, for applied frequencies of 520 and 700 kHz, only a few data points satisfied this condition (Figure 5B).

We selected the best performing sample of IONCs nanoparticles (19 nm in cube edge) for the cellular hyperthermia treatment. To this aim, the KB cells were grown in a 75 cm^2 culture flask until confluence was achieved. Then, the culture medium was replaced either with a solution of PC-IONCs or with a solution of PEG-IONCs at an administered concentration of 1 g/L in reference to iron. After incubation for 24 h at 37 °C, the cells did not show any sign of cell suffering; they were still confluent in the culture flask and were not detached, as observed under an optical microscope (Figure S5). The cell layer was scraped, and the cell pellet was washed three times, and finally, it was recovered and diluted to reach about 2×10^7 cells suspended in 300 μL of phosphate sodium buffer. The doped cell suspension was immediately tested in the hyperthermia setup, and the iron amount on the pellet was measured by elemental analysis.

For the cell study, we used a commercially available setup (magneTherm AC system Nanotherics Corp.) that reaches 110 kHz and 20 kAm^{-1}, which are conditions close to those applied so far on patients.[15] The heat treatment was applied for 1 h. Both the temperature and the percentage of dead cells, assessed by trypan blue assay, were recorded after treatment and plotted as a function of the total amount of iron associated with the pellet. Different trials were performed with different IONC preparations, the latter always administered to the cells at 1 g/L of iron (Figure 6). As a general trend, the total iron amount contained in the cell suspension affected the equilibrium temperature measured at the end of the treatment: it increased by increasing the amount of iron associated with the cells. It is important to remark that a significant variability between different cell experiments was found even if the amount of the administered iron was always fixed at 1 g/L for all of the experiments. This behavior is most likely due to the variability on cell growth cultured in 2D and to the variability of the stability in cell culture media of the different IONC batches used in the various experiments. It was found that after 1 h of treatment, in order to measure a temperature in the range between 40 and 45 °C (which is considered high enough for therapeutic purposes), an amount of iron associated with cells between 2 and 4 g/L was needed in our case. The percentage of dead cells measured followed a linear trend with respect to the total iron amount associated with the pellet. In the temperature range between 40 and 45 °C, cell mortalities around 45−50% were measured. It is also worth mentioning that when a higher nanoparticle concentration was associated with the pellet (iron concentration >5 g/L), even 100% mortality was observed after 1 h of treatment, likely because the cell suspension could be warmed to 65 °C at this concentration.

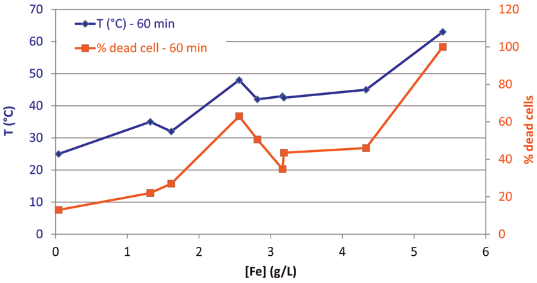

Figure 6. Temperature and viability curves after hyperthermia treatment. The blue curve correlates the concentration of iron in the cellular suspension with the equilibrium temperature measured after 60 min of treatment, at 110 kHZ and 20 kAm^{-1} (25 mT). The red curve correlates to the iron concentration in suspension with the percentage of dead cells after 60 min of hyperthermia exposure. The differences in iron concentration between the experimental points can be ascribed either to the number of cells or to the amount of IONCs associated with the cell pellet.

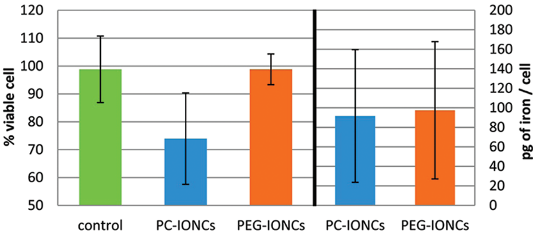

Figure 7. Cytotoxicity test for PC-IONCs or PEG-IONCs. In the left panel, trypan blue viability assay results are reported for KB cells after incubation with IONC suspension, for 24 h at the concentration (of iron) of 1 g/L. The higher cytotoxicity recorded for the polymer-coated sample might be likely attributed to a partial flocculation of the PC-IONC sample in the cellular medium during the incubation. In the case of PEG-IONCs, no precipitation was observed. In the right panel, the amounts of iron per cell (in pg) determined by elemental analysis are reported for the two samples. These values provide an indication of the amount of iron internalized and/or adsorbed onto the cellular membrane. The iron contents were estimated by ICP-AES measurements of treated cells. All points have been acquired in triplicate.

We have also normalized the total amount of iron measured by elemental analysis (via ICP) to each cell when either PC-IONCs or PEG-IONCs were administered to the cells at the external concentration of 1 g/L (Figure 7). Both types of nanocrystals were taken up in an equal amount, which corresponded to about less than 100 picograms (pg) of iron per cell, although the ICP data estimate the total amount of iron and do not provide any information on the localization of nanoparticles into the cells. It is not straightforward to compare the iron uptake with other reported studies. Indeed, the iron amount detected per cell could vary

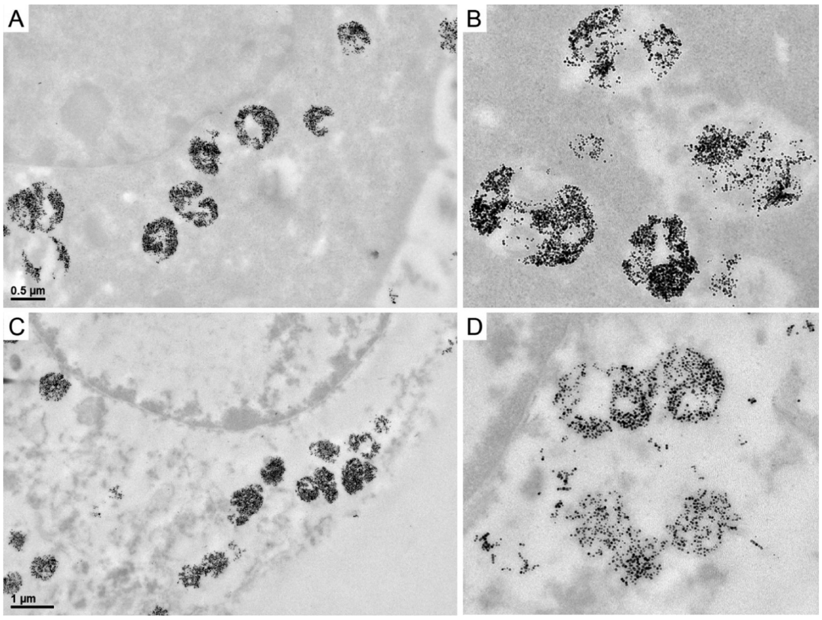

Figure 8. TEM characterization of treated cells. Micrographs of KB cells incubated with PEG-IONCs before (A,B) and after (C,D) hyperthermia treatment. Before treatment, the IONCs were organized in large endosomes within the cellular cytoplasm. In panel B, the KB cells were doped in the same conditions and treated for 1 h at 110 kHz and 20 kAm^{-1}. The global cellular structure was still recognizable, and the IONC aggregations were still present, but the cytoplasm and the nucleus were clearly damaged from the exposure to the temperature of 43 °C reached after 1 h of treatment.

from a few picograms to more than a hundred picograms, and it is strongly affected by the nanoparticle coating layer (dextran, citrate, polymer, *etc.*) and to potential aggregation of nanoparticles on cells,[46−49] the cell lineage used in the experiment[49,50] and the iron dosage administrated.[50,51] In our case, the main difference between PC-IONCs and PEG-IONCs was in their cytotoxicities assessed by the trypan blue test. At 1 g/L doping concentration, in the case of PC-IONCs, the viability of the cells was reduced down to 70%, while in the case of PEG-IONCs, no significant reduction of cell viability was measured, and the viability was assessed to be 100% as for the control cell sample. This difference is likely ascribed to the different stability of those IONCs in the cell media. It was indeed observed that, after 24 h, the PC-IONCs had formed large aggregates on top of the cell layers, while the PEG-IONCs were more homogeneously distributed on top of the cell layer. Despite the fact that PEG molecules should reduce the nonspecific uptake of IONCs, we did not observe this difference when measuring the intracellular iron amount, which is likely due to the large excess of IONC concentration administered to the cells (1 g/L) and additionally to some degree of aggregation occurring in the cell medium after an incubation time of 24 h. Nevertheless, the high intracellular iron concentration associated with the cell pellet could mimic the tumor mass volume *in vivo* and allow us to observe how the IONCs behave.

We have also looked at the effects of hyperthermia operated by the cube-shaped IONCs on the KB cells. By TEM characterization performed on KB cells doped with PEG-IONCs, it was possible to observe a high level of internalization of the IONCs (Figure 8A). The nanoparticles (before the treatment) were located mostly in large and dense endosomes but also on the cellular membrane. After 1 h of hyperthermia treatment (Figure 8C), the cell morphology was drastically modified: the organelles and the cytoplasmic structures were losing their organization, and the nucleic acid started to condense in large agglomerates within the nuclei. In addition, the nuclear membrane was damaged or disrupted while the IONCs were still present inside the cells. All of those morphological cell changes indicate that the advanced necrosis process had been activated.

The *in vitro* results as a whole allow one to assess that the cube-shaped IONCs, once internalized by the cells, are still able to heat up and damage the cells and thus they are still functional as heating probes.

If we compare the SAR values recorded on cube-shaped IONCs of 19 nm with the SAR data so far reported, we can assess that our values are among the highest recorded for iron oxide nanocrystals.[16,37] Recently, remarkably large SAR values have been reported by combining different magnetic core−shell structures. For instance, SAR values of around 2200 W/g have been measured for 15 nm $CoFe_2O_4@MnFe_2O_4$ nanoparticles at 500 kHz and 37.3 kAm^{-1}.[13] By fitting our experimental data with a square law (see Supporting Information), it is possible to extrapolate the SAR values for those conditions for the 19 nm IONCs. The results of the fit indicate a SAR value of about 4200 W/g$_{Fe}$ (or 2940 W/g if referred to one gram of magnetic material). It is also important to remark that the SAR values recorded in our work have been achieved with iron-based nanocrystals and no potential toxic elements are included in these particles. Concerning this issue, very large SARs were also recorded on metallic iron NPs having a cube shape; however, those NPs are not ready yet for biomedical applications since they need to be protected from oxidation and their toxicity has not yet been studied.[52]

Our SAR values are in the same range as those recorded on magnetosomes extracted from AMB-1 magnetotactic bacteria.[53] On magnetosomes, Alphandery found a SAR value of 875 W/g_{Fe} at 183 kHz and 32 kAm^{-1}, corresponding to an *Hf* factor of 5×10^9 kAm^{-1} s^{-1}, while for our 19 nm IONCs, we found a SAR of 509 W/g_{Fe} at 320 kHz and 15 kAm^{-1}, corresponding to an *Hf* factor of 4.8×10^9 kAm^{-1} s^{-1}. For magnetosomes, it is also worth mentioning that some critical issues need to be overcome, such as the isolation of individual magnetosomes from the chain produced by the bacteria (without compromising the stability and SAR of the magnetosomes) and the minimization of the immune response originated by the use of a bacterial product.[35]

CONCLUSIONS

In this work, we have studied the hyperthermia performance of samples of cube-shaped IONCs of various cube edge lengths, which were prepared by thermal decomposition using a one-pot synthesis approach. The initial IONCs had high saturation magnetization and significant coercive field, which were maintained once transferred in water by coating them with an amphiphilic polymer. The SAR values recorded at different frequencies and magnetic field amplitudes for the different IONC sizes revealed that the 19 nm sample had the best performance at all conditions tested. The square dependence of the SAR as a function of the magnetic field amplitude and the linear dependence of the SAR values recorded as a function of the frequency allowed us to assess that, in order to achieve higher efficient hyperthermia treatment by using the same amount of magnetic nanoparticles, it is advisible to apply lower frequencies and higher magnetic field amplitudes. From the technical point of view, this represents an advantage as it is easier to apply a higher magnetic field amplitude at a lower frequency. It is also worth underlining that significant SAR values have been achieved for these cube-shaped IONCs at frequency and magnetic field conditions that are considered biomedically safe.

Furthermore, hyperthermia experiments performed on tumor KB cells by employing the 19 nm cube-shaped IONCs allowed us to assess that these nanocrystals are still able to function as heat probes at 110 kHz and 20 kAm^{-1}, even when internalized by the cells in endosomal compartments. Additionally, with these nanoparticles, the amount of iron necessary to reach an equilibrium temperature in the range between 40 and 45 °C (which is considered the appropriate temperature range to obtain a therapeutic effect) was estimated at 4 g/L, which might be useful for reducing the *in vivo* dose of IONC needed: so far, to reach *in vivo* the same temperature, 2 orders of magnitude more material have been used.[15,54] For the cube-shaped IONCs exhibiting this heating effect, a corresponding *in vitro* mortality attested around 50% was estimated after 1 h of treatment, with corresponding necrotic damage to the cells. As a next step, *in vivo* animal tests are under investigation in order to establish their efficacy on a tumor model.

EXPERIMENTAL SECTION

Chemicals. Iron(III) acetylacetonate (99%), decanoic acid (99%), and dibenzyl ether (99%) were purchased from Acros. Poly(maleic anhydride-*alt*-1-octadecene), methoxypolyethylene glycol amine (PEG750), *N*-(3-dimethylaminopropyl)-*N*′-ethylcarbodiimide hydrochloride (EDC), fetal bovine serum (FBS), glutamine, penicillin/streptomycin, glutaraldehyde, sodium cacodylate trihydrate, osmium tetroxide, and epoxy resin were purchased from Sigma-Aldrich. RPMI-1640 without folic acid was purchased from Euroclone. Milli-Q water (18.2 MΩ, filtered with filter pore size 0.22 μM) was from Millipore. All solvents used were of analytical grade and were purchased from Sigma-Aldrich. All chemicals were used as received.

Synthesis of Iron Oxide Nanocubes. All experiments were carried out in a standard Schlenk line using 25 mL three-neck (14/23) round-bottom flasks connected to water-cooled Allin condensers. The synthesis of iron oxide nanocubes over a wide range of sizes is not straightforward. The experimental conditions reported here should be taken as a starting point, then many parameters influence the final size and shape. In our case, the following conditions were the most suitable ones for synthesizing cubes of 12, 19, 25, and 38 nm.

12 nm particles: To synthesize small cube-shaped IONCs of about 12 nm in edge length (see Figure 1A), 0.353 g (1 mmol) of iron(III) acetylacetonate was mixed with 0.69 g (4 mmol) of decanoic acid in 25 mL of dibenzyl ether. After degassing for 1 h at 60 °C, the solution was heated to 200 °C (at a rate of 5 °C/min) under argon with vigorous stirring. After 2.5 h at 200 °C, the solution was heated to reflux temperature at a heating rate of 10 °C/min and kept at this temperature for 1 h. After cooling to room temperature, 60 mL of acetone was added and the whole solution was centrifuged at 8500 rpm. After removing the supernatant, the black precipitate was dispersed in 2−3 mL of chloroform and the washing procedure was repeated at least two more times. Finally, the collected particles were dispersed in 15 mL of chloroform.

19 nm particles: To synthesize iron oxide nanocubes of about 19 nm in edge length (Figure 1B), 0.353 g (1 mmol) of iron(III) acetylacetonate and 0.69 g (4 mmol) of decanoic acid were mixed in 25 mL of dibenzyl ether. After degassing at room temperature for 45 min, the solution was heated to 200 °C (5 °C/min) and kept at this temperature for 2.5 h. Finally, the temperature was increased to reflux temperature (at a rate of 10 °C/min) and kept at this value for 1 h. After cooling to room temperature, the particles were collected by adding a 4-fold

volume of acetone/chloroform and centrifuged at 8000 rpm. As for the 12 nm particles, the sample was washed three times and dispersed in 15 mL of chloroform.

25 nm particles: Larger nanocubes of about 25 nm in edge length (see Figure 1C) were obtained by slightly decreasing the molar ratio of the iron(III) acetylacetonate to decanoic acid as follows: 0.353 g (1 mmol) of iron(III) acetylacetonate, 0.69 g (4 mmol) of decanoic acid, and 25 mL of dibenzyl ether were mixed together in a 50 mL three-neck round-bottom flask. Following the same procedure as for 19 nm nanocubes, after degassing for 45 min at room temperature, the solution was heated to 200 °C and kept at this temperature for 2.5 h. In a second step, the solution was heated to reflux temperature (at a rate of 6 °C/min) and kept at this value for 1 h. The solution was always under an argon flow and under vigorous stirring. Particles were washed following the same procedure mentioned above and dispersed in 15 mL of chloroform.

38 nm particles: The largest particles of 38 nm in edge length (see Figure 1D) were synthesized by mixing 0.353 g (1 mmol) of iron(III) acetylacetonate with 0.69 g (4 mmol) of decanoic acid in 25 mL of dibenzyl ether. After degassing for 90 min at room temperature, the mixture was heated to 200 °C (at a rate of 15 °C/min) and kept at this value for 2.5 h. Finally, the temperature was increased at a heating rate of 4 °C/min until reflux and maintained at this value for 1 h. After cooling to room temperature, the particles were washed by following the above-mentioned procedure.

Hyperthermia Measurements. To evaluate the SAR of the IONCs, a homemade device was used. First, 300 μL of water-soluble IONC solution was introduced into a copper coil that was part of a resonant RLC homemade circuit capable of generating an AC magnetic field in the frequency range from 320 kHz up to 1.1 MHz and with magnetic field amplitude up to 28 kAm^{-1}. By circulating nonane into the coil, the temperature inside the sample holder was kept to 37 °C. A fluoro-optic thermometer fiber probe (Luxtron Corp., CA) was used to probe the temperature every 0.7 s after switching on the magnetic applied field. The major technical limitation of the device is represented by a restriction on the magnetic field amplitude for some of the frequencies, with 36 mT being the highest amplitude reached only for 520 kHz. All measurements, if not otherwise stated, were performed in water ($C_{\text{water}} = 4185$ J L^{-1} K^{-1}) and normalized by using the amount of iron evaluated by elemental analysis (g_{Fe}/L). All reported SAR values and error bars were calculated from the mean and standard deviation of at least four experimental measurements.

Magnetic Measurements. Characterization of the samples was carried out using a superconducting quantum interference device (SQUID) from Quantum Design. Magnetization curves were measured from 50 to +50 kOe at 300 K and also at 5 K upon zero field cooling (ZFC) and field cooling (FC) conditions. The thermal dependence of the magnetization of liquid samples was also measured upon ZFC and FC.

Polymer Coating of Single IONCs. The IONCs were transferred in water by using poly(maleic anhydride-*alt*-1-octadecene), as previously reported by some of us, with various modifications.[55] When the size of the nanocubes was of 10−13 nm, no modifications were applied to the standard protocol. When the particles had a diameter above 16 nm, some changes were introduced. In detail, a solution of poly(maleic anhydride-*alt*-1-octadecene) in chloroform was added to a solution of surfactant-coated nanocrystals in chloroform, at a concentration of 0.01 μM, in order to reach a ratio of polymer monomer units per square nanometers of nanocrystal surface equal to 500. The solution was then sonicated for 10 min. Soon after, the solvent was slowly evaporated by two steps: first, the solution was kept at 60 °C and 980 mbar for 10 min; soon after, the temperature was raised to 70 °C (keeping the pressure set to 980 mbar) and the solvent was slowly evaporated. After this step, a solution of cross-linker, bis(hexamethylene)triamine in chloroform, was added to reach a ratio of cross-linker molecules per square nanometer of nanocrystal surface equal to 10 (the latter step, however, is considered optional and can also be skipped without compromising the nanoparticle water solubility). Chloroform was added to the solution to reach a final concentration of nanoparticles of about 0.2 μM. After sonicating the sample for 30 min at room temperature, the solvent was again removed under controlled pressure (using a rotavapor, at 40 °C and 350 mbar). The cross-linking step is considered optional and can also be skipped. A thin film of nanoparticles collected on the walls of the flask indicated the complete removal of the solvent. Sodium borate buffer (50 mM, pH 9) was added until it covered the solid layer of nanoparticles in the reaction flask, and the resulting mixture was sonicated until the polymeric film could be detached entirely from the flask wall. Then, the solution was ultrasonicated for 20 min in order to allow the complete transfer in water of the particles. The solution was then filtered on syringe filters (0.22 μm pore sizes) in order to remove possible large aggregates. The solution was concentrated on a centrifuge tube equipped with a cellulose membrane (Amicon Ultra-135, Millipore) and purified on 20−66% continuous sucrose gradient, as reported in the previous protocol.[55]

PEG Coating. After polymer coating, the IONCs used in the cellular hyperthermia test were coated with a layer of methoxypolyethylene glycol amine (PEG750). The coating was performed by applying an established protocol,[56] with minor modifications. Briefly, a solution of IONCs of 19 nm in size, at a concentration of 6×10^{-7} M, was reacted with equal volumes of PEG750 (6×10^{-4} M) and EDC (1.5×10^{-1} M) for 3 h. All of the solutions had been freshly prepared in 50 mM sodium borate buffer. After the reaction, the IONCs were washed five times on a centrifuge tube equipped with a cellulose membrane and filtered on 0.22 μm syringe filters before being administered to cellular monolayer. It is worth mentioning that PEG-coated IONCs were colloidally stable in the cell culture medium, while the PC-coated IONCs tended to flocculate.

Cell Culture. The human epidermoid carcinoma cells, known as KB cells (ATCC #CCL-17), were grown continuously as a monolayer at 37 °C and under 5% CO_2 atmosphere in RPMI-1640 medium (folic-acid-free) supplemented with L-glutamine (2 mL), penicillin (100 units/mL), streptomycin (100 μg/mL), and 10% heat-inactivated fetal bovine serum (FBS).

Hyperthermia Experiments Performed on Cells. KB cell were grown up to a confluent state in a 75 cm^2 culture flask.[57] The culture medium was replaced with 5 mL of either PC-IONCs or PEG-IONCs dispersed in RPMI-1640 (supplemented with 10% of FBS), at a concentration of 1 g/L of iron. After 24 h, the doping medium was removed and the cell layer was washed five times with PBS, detached with a scraper, and washed three more times by centrifugation. The cellular pellet was then transferred in a sample vial, yielding a cellular suspension of 2×10^7 KB cell in 300 μL of PBS. The cells were finally tested in a hyperthermia setup, by applying an alternating magnetic field at a frequency of 110 kHz and at a magnetic field amplitude of 20 kAm^{-1} for 1 h. The hyperthermia measurements in this case were performed by using a magneTherm AC system (Nanotherics Corp.). All experiments were carried out far below the biological limit by using an applied field of 20 kAm^{-1} and a frequency of 110 kHz ($Hf = 2.2 \times 10^9$ $\text{A}\cdot\text{m}^{-1}\cdot\text{s}^{-1}$). A fluoro-optic thermometer fiber probe (Luxtron Corp., CA) was used to probe the temperature every 0.25 s after switching on the magnetic applied field.

Viability Test. In order to avoid possible interferences caused by adsorbed IONCs onto the cells' surface, the viability test known as "trypan blue staining" was applied to assess the number of live/dead cells, before and after the hyperthermia treatment. After the staining, the cells were counted on the Buerker chamber, following the standard protocol.

Transmission Electron Microscopy (TEM). TEM images were recorded with a JEOL JEM 1011 microscope operating at an accelerating voltage of 100 kV. For the characterization of the doped cells, after the incubation with IONCs, the KB cells (1×10^6) were washed three times in 0.1 M cacodylate buffer and fixed with 2.5% glutaraldehyde in cacodylate buffer at 4 °C for 30 min. The fixed cells were washed three times with cacodylate buffer, and then 1% osmium tetroxide in cacodylate buffer was added for 1 h at room temperature. After another three washing steps in cacodylate buffer, the cells were dehydrated with 30, 50, 75, 85, 95, and 100% (three times) absolute ethanol. Thereafter, the cells were infiltrated with Epon resin (two steps: 50 and 66% for resin in absolute ethanol, 30 min each) and embedded in 100% resin at 60 °C for 2 days.

Ultrathin sections (70 nm thick) were cut on an Ultramicrotome (Leika), stained with lead citrate, and observed by TEM.

Elemental Analysis. The concentration of iron was determined by elemental analysis using an ICP-AES spectrometer (iCAP 6500, Thermo). The samples were digested in concentrated 3:1 HCl/HNO_3 (v/v) solutions.

Gel Electrophoresis. Electrophoretic characterization was carried out on 1% agarose gel for a run time of 1 h at 100 V, after which the gel was observed in bright field. Each sample had been supplemented with glycerol (20%) before the loading step.

Dynamic Light Scattering Measurements. Dynamic light scattering (DLS) measurements were performed using a Zeta Sizer (Malvern Instruments) equipped with a 4.0 mW He–Ne laser operating at 633 nm and an Avalanche photodiode detector.

Conflict of Interest: The authors declare no competing financial interest.

Acknowledgment. This work was supported by the European project Magnifyco (Contract NMP4-SL-2009-228622). We thank Simone Nitti and Giammarino Pugliese for help with the nanoparticle preparation, Roberta Ruffilli for help with cell sectioning for TEM observation, and Dr. Miguel Angel Garcia and Dr. Albert Figuerola for helpful discussions on the magnetic measurements.

Supporting Information Available: Addional details and figures. This material is available free of charge *via* the Internet at http://pubs.acs.org.

REFERENCES AND NOTES

1. Bruns, O. T.; Ittrich, H.; Peldschus, K.; Kaul, M. G.; Tromsdorf, U. I.; Lauterwasser, J.; Nikolic, M. S.; Mollwitz, B.; Merkel, M.; Bigall, N. C. Real-Time Magnetic Resonance Imaging and Quantification of Lipoprotein Metabolism *in Vivo* Using Nanocrystals. *Nat. Nanotechnol.* **2009**, *4*, 193–201.
2. Pankhurst, Q. A.; Thanh, N. K. T.; Jones, S. K.; Dobson, J. Progress in Applications of Magnetic Nanoparticles in Biomedicine. *J. Phys. D: Appl. Phys.* **2009**, *42*, 224001.
3. Gupta, A. K.; Gupta, M. Synthesis and Surface Engineering of Iron Oxide Nanoparticles for Biomedical Applications. *Biomaterials* **2005**, *26*, 3995–4021.
4. Mornet, S.; Vasseur, S.; Grasset, F.; Duguet, E. Magnetic Nanoparticle Design for Medical Diagnosis and Therapy. *J. Mater. Chem.* **2004**, *14*, 2161–2175.
5. Hergt, R.; Dutz, S.; Müller, R.; Zeisberger, M. Magnetic Particle Hyperthermia: Nanoparticle Magnetism and Materials Development for Cancer Therapy. *J. Phys.: Condens. Matter* **2006**, *18*, S2919.
6. Roti Roti, J. L. Cellular Responses to Hyperthermia (40–46°C): Cell Killing and Molecular Events. *Int. J. Hyperthermia* **2008**, *24*, 3–15.
7. Franconi, C.; Vrba, J.; Micali, F.; Pesce, F. Prospects for Radiofrequency Hyperthermia Applicator Research. I – Pre-Optimised Prototypes of Endocavitary Applicators with Matching Interfaces for Prostate Hyperplasia and Cancer Treatments. *Int. J. Hyperthermia* **2011**, *27*, 187–198.
8. Sullivan, D. M.; Ben-Yosef, R.; Kapp, D. S. Stanford 3D Hyperthermia Treatment Planning System. Technical Review and Clinical Summary. *Int. J. Hyperthermia* **1993**, *9*, 627–643.
9. Leybovicht, L. B.; Myerson, R. J.; Emami, B.; Straube, W. L. Evaluation of the Sigma 60 Applicator for Regional Hyperthermia in Terms of Scattering Parameters. *Int. J. Hyperthermia* **1991**, *7*, 917–935.
10. Rosensweig, R. E. Heating Magnetic Fluid with Alternating Magnetic Field. *J. Magn. Magn. Mater.* **2002**, *252*, 370–374.
11. Glöckl, G.; Hergt, R.; Zeisberger, M.; Dutz, S.; Nagel, S.; Weitschies, W. The Effect of Field Parameters, Nanoparticle Properties and Immobilization on the Specific Heating Power in Magnetic Particle Hyperthermia. *J. Phys.: Condens. Matter* **2006**, *18*, S2935.
12. Hergt, R.; Dutz, S. Magnetic Particle Hyperthermia-Biophysical Limitations of a Visionary Tumour Therapy. *J. Magn. Magn. Mater.* **2007**, *311*, 187–192.
13. Lee, J.-H.; Jang, J.-T.; Choi, J.-S.; Moon, S. H.; Noh, S.-H.; Kim, J.-W.; Kim, J.-G.; Kim, I.-S.; Park, K. I.; Cheon, J. Exchange-Coupled Magnetic Nanoparticles for Efficient Heat Induction. *Nat. Nanotechnol.* **2011**, *6*, 418–422.
14. Thiesen, B.; Jordan, A. Clinical Applications of Magnetic Nanoparticles for Hyperthermia. *Int. J. Hyperthermia* **2008**, *24*, 467–474.
15. Maier-Hauff, K.; Rothe, R.; Scholz, R.; Gneveckow, U.; Wust, P.; Thiesen, B.; Feussner, A.; Deimling, A.; Waldoefner, N.; Felix, R. Intracranial Thermotherapy Using Magnetic Nanoparticles Combined with External Beam Radiotherapy: Results of a Feasibility Study on Patients with Glioblastoma Multiforme. *J. Neuro-Oncol.* **2007**, *81*, 53–60.
16. Fortin, J. P.; Wilhelm, C.; Servais, J.; Ménager, C.; Bacri, J. C.; Gazeau, F. Size-Sorted Anionic Iron Oxide Nanomagnets as Colloidal Mediators for Magnetic Hyperthermia. *J. Am. Chem. Soc.* **2007**, *129*, 2628–2635.
17. Hergt, R.; Hiergeist, R.; Hilger, I.; Kaiser, W. A.; Lapatnikov, Y.; Margel, S.; Richter, U. Maghemite Nanoparticles with Very High AC-Losses for Application in RF-Magnetic Hyperthermia. *J. Magn. Magn. Mater.* **2004**, *270*, 345–357.
18. Natividad, E.; Castro, M.; Mediano, A. Accurate Measurement of the Specific Absorption Rate Using a Suitable Adiabatic Magnetothermal Setup. *Appl. Phys. Lett.* **2008**, *92*, 093116–3.
19. Kovalenko, M. V.; Bodnarchuk, M. I.; Lechner, R. T.; Hesser, G.; Schäffler, F.; Heiss, W. Fatty Acid Salts as Stabilizers in Size- and Shape-Controlled Nanocrystal Synthesis: The Case of Inverse Spinel Iron Oxide. *J. Am. Chem. Soc.* **2007**, *129*, 6352–6353.
20. Klokkenburg, M.; Vonk, C.; Claesson, E. M.; Meeldijk, J. D.; Erné, B. H.; Philipse, A. P. Direct Imaging of Zero-Field Dipolar Structures in Colloidal Dispersions of Synthetic Magnetite. *J. Am. Chem. Soc.* **2004**, *126*, 16706–16707.
21. Hergt, R.; Hiergeist, R.; Zeisberger, M.; Schüler, D.; Heyen, U.; Hilger, I.; Kaiser, W. A. Magnetic Properties of Bacterial Magnetosomes as Potential Diagnostic and Therapeutic Tools. *J. Magn. Magn. Mater.* **2005**, *293*, 80–86.
22. Neuberger, T.; Schöpf, B.; Hofmann, H.; Hofmann, M.; Von Rechenberg, B. Superparamagnetic Nanoparticles for Biomedical Applications: Possibilities and Limitations of a New Drug Delivery System. *J. Magn. Magn. Mater.* **2005**, *293*, 483–496.
23. Figuerola, A.; Di Corato, R.; Manna, L.; Pellegrino, T. From Iron Oxide Nanoparticles towards Advanced Iron-Based Inorganic Materials Designed for Biomedical Applications. *Pharmacol. Res.* **2010**, *62*, 126–143.
24. Hilger, I.; Hergt, R.; Kaiser, W. A. Use of Magnetic Nanoparticle Heating in the Treatment of Breast Cancer. *IEE Proc. Nanobiotechnol.* **2005**, *152*, 33–39.
25. Fortin, J. P.; Gazeau, F.; Wilhelm, C. Intracellular Heating of Living Cells through Néel Relaxation of Magnetic Nanoparticles. *Eur. Biophys. J.* **2008**, *37*, 223–228.
26. Martinez-Boubeta, C.; Balcells, L.; Cristòfol, R.; Sanfeliu, C.; Rodríguez, E.; Weissleder, R.; Lope-Piedrafita, S.; Simeonidis, K.; Angelakeris, M.; Sandiumenge, F. Self-Assembled Multifunctional Fe/MgO Nanospheres for Magnetic Resonance Imaging and Hyperthermia. *Nanomedicine* **2010**, *6*, 362–370.
27. Kappiyoor, R.; Liangruksa, M.; Ganguly, R.; Puri, I. K. The Effects of Magnetic Nanoparticle Properties on Magnetic Fluid Hyperthermia. *J. Appl. Phys.* **2010**, *108*, 094702-8.
28. Habib, A. H.; Ondeck, C. L.; Chaudhary, P.; Bockstaller, M. R.; McHenry, M. E. Evaluation of Iron-Cobalt/Ferrite Core–Shell Nanoparticles for Cancer Thermotherapy. *J. Appl. Phys.* **2008**, *103*, 07A307-3.
29. Jordan, A.; Scholz, R.; Wust, P.; Fähling, H.; Krause, J.; Wlodarczyk, W.; Sander, B.; Vogl, T.; Felix, R. Effects of Magnetic Fluid Hyperthermia (MFH) on C3H Mammary Carcinoma *in Vivo*. *Int. J. Hyperthermia* **1997**, *13*, 587–605.
30. Sonvico, F.; Mornet, S.; Vasseur, S.; Dubernet, C.; Jaillard, D. Degrouard, J.; Hoebeke, J.; Duguet, E.; Colombo, P.; Couvreur, P. Folate-Conjugated Iron Oxide Nanoparticles for Solid Tumor Targeting as Potential Specific Magnetic Hyperthermia Mediators: Synthesis, Physicochemical Characterization,

and *In Vitro* Experiments. *Bioconjugate Chem.* **2005**, *16*, 1181–1188.

31. Massart, R. Preparation of Aqueous Magnetic Liquids in Alkaline and Acid Media. *IEEE Trans. Magn.* **1981**, *17*, 1247–1248.
32. Guardia, P.; Batlle-Brugal, B.; Roca, A. G.; Iglesias, O.; Morales, M. P.; Serna, C. J.; Labarta, A.; Batlle, X. Surfactant Effects in Magnetite Nanoparticles of Controlled Size. *J. Magn. Magn. Mater.* **2007**, *316*, e756–e759.
33. Sugimoto, T.; Matijevic, E. Formation of Uniform Spherical Magnetite Particles by Crystallization from Ferrous Hydroxide Gels. *J. Colloid Interface Sci.* **1980**, *74*, 227–243.
34. Bazylinski, D. A.; Frankel, R. B. Magnetosome Formation in Prokaryotes. *Nat. Rev. Microbiol.* **2004**, *2*, 217–230.
35. Alphandéry, E.; Faure, S.; Raison, L.; Duguet, E.; Howse, P. A.; Bazylinski, D. A. Heat Production by Bacterial Magnetosomes Exposed to an Oscillating Magnetic Field. *J. Phys. Chem. C* **2011**, *115*, 18–22.
36. Pérez, N.; Bartolomé, F.; García, L. M.; Bartolome, J.; Morales, M. P.; Serna, C. J.; Labarta, A.; Batlle, X. Nanostructural Origin of the Spin and Orbital Contribution to the Magnetic Moment in $Fe_{3-x}O_4$ Magnetite Nanoparticles. *Appl. Phys. Lett.* **2009**, *94*, 093108-3.
37. Lartigue, L.; Innocenti, C.; Kalaivani, T.; Awwad, A.; Sanchez Duque, M. d. M.; Guari, Y.; Larionova, J.; Guérin, C.; Montero, J.-L. G.; Barragan-Montero, V. Water-Dispersible Sugar-Coated Iron Oxide Nanoparticles. An Evaluation of Their Relaxometric and Magnetic Hyperthermia Properties. *J. Am. Chem. Soc.* **2011**, *133*, 10459–10472.
38. Yu, W. W.; Falkner, J. C.; Yavuz, C. T.; Colvin, V. L. Synthesis of Monodisperse Iron Oxide Nanocrystals by Thermal Decomposition of Iron Carboxylate Salts. *Chem. Commun.* **2004**, 2306–2307.
39. Sun, S.; Zeng, H.; Robinson, D. B.; Raoux, S.; Rice, P. M.; Wang, S. X.; Li, G. Monodisperse MFe_2O_4 (M = Fe, Co, Mn) Nanoparticles. *J. Am. Chem. Soc.* **2004**, *126*, 273–279.
40. Hou, Y.; Xu, Z.; Sun, S. Controlled Synthesis and Chemical Conversions of FeO Nanoparticles. *Angew. Chem., Int. Ed.* **2007**, *46*, 6329–6332.
41. Levy, M.; Quarta, A.; Espinosa, A.; Figuerola, A.; Wilhelm, C.; García-Hernández, M.; Genovese, A.; Falqui, A.; Alloyeau, D.; Buonsanti, R.; *et al.* Correlating Magneto-Structural Properties to Hyperthermia Performance of Highly Monodisperse Iron Oxide Nanoparticles Prepared by a Seeded-Growth Route. *Chem. Mater.* **2011**, *23*, 4170–4180.
42. Guardia, P.; Pérez-Juste, J.; Labarta, A.; Batlle, X.; Liz-Marzán, L. M. Heating Rate Influence on the Synthesis of Iron Oxide Nanoparticles: The Case of Decanoic Acid. *Chem. Commun.* **2010**, *46*, 6108–6110.
43. Pellegrino, T.; Manna, L.; Kudera, S.; Liedl, T.; Koktysh, D.; Rogach, A. L.; Keller, S.; Rädler, J.; Natile, G.; Parak, W. J. Hydrophobic Nanocrystals Coated with an Amphiphilic Polymer Shell: A General Route to Water Soluble Nanocrystals. *Nano Lett.* **2004**, *4*, 703–707.
44. Guardia, P.; Perez, N.; Labarta, A.; Batlle, X. Controlled Synthesis of Iron Oxide Nanoparticles over a Wide Size Range. *Langmuir* **2009**, *26*, 5843–5847.
45. Goya, G. F.; Berquó, T. S.; Fonseca, F. C.; Morales, M. P. Static and Dynamic Magnetic Properties of Spherical Magnetite Nanoparticles. *J. Appl. Phys.* **2003**, *94*, 3520–3528.
46. Kalambur, V. S.; Longmire, E. K.; Bischof, J. C. Cellular Level Loading and Heating of Superparamagnetic Iron Oxide Nanoparticles. *Langmuir* **2007**, *23*, 12329–12336.
47. Safi, M.; Courtois, J.; Seigneuret, M.; Conjeaud, H.; Berret, J. F. The Effects of Aggregation and Protein Corona on the Cellular Internalization of Iron Oxide Nanoparticles. *Biomaterials* **2011**, *32*, 9353–9363.
48. Huang, C.; Neoh, K. G.; Wang, L.; Kang, E.-T.; Shuter, B. Magnetic Nanoparticles for Magnetic Resonance Imaging: Modulation of Macrophage Uptake by Controlled Pegylation of the Surface Coating. *J. Mater. Chem.* **2010**, *20*, 8512–8520.
49. Zhang, Y.; Kohler, N.; Zhang, M. Surface Modification of Superparamagnetic Magnetite Nanoparticles and Their Intracellular Uptake. *Biomaterials* **2002**, *23*, 1553–1561.
50. Liu, Y.; Chen, Z.; Wang, J. Systematic Evaluation of Biocompatibility of Magnetic Fe_3O_4 Nanoparticles with Six Different Mammalian Cell Lines. *J. Nanopart. Res.* **2011**, *13*, 199–212.
51. Luciani, N.; Gazeau, F.; Wilhelm, C. Reactivity of the Monocyte/Macrophage System to Superparamagnetic Anionic Nanoparticles. *J. Mater. Chem.* **2009**, *19*, 6373–6380.
52. Mehdaoui, B.; Meffre, A.; Lacroix, L. M.; Carrey, J.; Lachaize, S.; Gougeon, M.; Respaud, M.; Chaudret, B. Large Specific Absorption Rates in the Magnetic Hyperthermia Properties of Metallic Iron Nanocubes. *J. Magn. Magn. Mater.* **2010**, *322*, L49–L52.
53. Alphandéry, E.; Faure, S.; Seksek, O.; Guyot, F.; Chebbi, I. Chains of Magnetosomes Extracted from AMB-1 Magnetotactic Bacteria for Application in Alternative Magnetic Field Cancer Therapy. *ACS Nano* **2011**, *5*, 6279–6296.
54. Gazeau, F.; Lévy, M.; Wilhelm, C. Optimizing Magnetic Nanoparticle Design for Nanothermotherapy. *Nanomedicine* **2008**, *3*, 831–844.
55. Di Corato, R.; Quarta, A.; Piacenza, P.; Ragusa, A.; Figuerola, A.; Buonsanti, R.; Cingolani, R.; Manna, L.; Pellegrino, T. Water Solubilization of Hydrophobic Nanocrystals by Means of Poly(maleic anhydride-*alt*-1-octadecene). *J. Mater. Chem.* **2008**, *18*, 1991–1996.
56. Sperling, R. A.; Pellegrino, T.; Li, J. K.; Chang, W. H.; Parak, W. J. Electrophoretic Separation of Nanoparticles with a Discrete Number of Functional Groups. *Adv. Funct. Mater.* **2006**, *16*, 943–948.
57. Wilhelm, C.; Fortin, J. P.; Gazeau, F. Tumour Cell Toxicity of Intracellular Hyperthermia Mediated by Magnetic Nanoparticles. *J. Nanosci. Nanotechnol.* **2007**, *7*, 2933–2937.